

A Python Calculator for Supernova Remnant Evolution

D.A. Leahy and J.E. Williams

Department of Physics & Astronomy, University of Calgary, Calgary, Alberta T2N 1N4,
Canada

Received _____; accepted _____

arXiv:1701.05942v2 [astro-ph.HE] 24 Jan 2017

ABSTRACT

A freely available Python code for modelling SNR evolution has been created. This software is intended for two purposes: to understand SNR evolution; and to use in modelling observations of SNR for obtaining good estimates of SNR properties. It includes all phases for the standard path of evolution for spherically symmetric SNRs. In addition, alternate evolutionary models are available, including evolution in a cloudy ISM, the fractional energy loss model, and evolution in a hot low-density ISM. The graphical interface takes in various parameters and produces outputs such as shock radius and velocity vs. time, SNR surface brightness profile and spectrum. Some interesting properties of SNR evolution are demonstrated using the program.

Subject headings: supernova remnants:

1. Introduction

The study of supernova remnants (SNRs) is of great interest in astrophysics (see Vink (2012) and references therein for a recent review). SNRs provide valuable information relevant to stellar evolution, the evolution of the Galaxy and its interstellar medium. SNRs are the dominant source of kinetic energy input into the interstellar medium.

SNRs are observed primarily in X-rays, by emission from hot interior gas with temperature ~ 1 keV, and in radio, by synchrotron emission from relativistic electrons accelerated by the SNR shockwave. The observational constraints for different SNRs are often different in nature. They depend on the brightness of emissions in different wavebands by a given SNR and by the instruments used to observe that SNR. Only a small fraction of the ~ 300 observed SNRs in our Galaxy have been well enough characterized to determine their evolutionary state, including explosion type, explosion energy and age. In order to expedite characterization of SNRs, we present a set of SNR models and a software implementation in Python.

The set of models consists of a wide set of models constructed previously by other authors (details given below). We carry out the additional step of consistently joining different stages of evolution, which in many cases has not been done before. The resulting software facilitates the process of using different constraints from observations to obtain SNR physical properties of interest.

The structure of the paper is as follows. Section 2 presents an overview of supernova remnant evolution. Section 3.1 describes some of the overall properties related to calculation of SNR models, such as characteristic time and radius scales and electron-ion temperature equilibration. Section 3.2 describes the calculations for the standard evolutionary path of a SNR. Section 3.3 describes alternate evolutionary paths, including cases of SNR in a cloudy ISM, the fractional energy loss model for SNR, and SNR evolution in a hot low-density ISM.

Section 3.4 briefly describes the software. Section 4 gives results from example calculations done with the software and Section 5 gives a brief summary.

2. Overview of Supernova Remnant Evolution

A supernova (SN) explosion creates a SNR starting with the ejection of the SN progenitor envelope at high speed, typically 5000-10000 km/s. General descriptions of SNR evolution are given in numerous places (e.g. see Cioffi et al. (1988) and Truelove & McKee (1999), hereafter referred to as TM99). In the case where a compact remnant is formed, the envelope is the progenitor less the core that becomes the remnant. In the case of no remnant, such as for thermonuclear Type Ia explosions, the ejected mass (envelope) is the entire SN progenitor. The high-speed ejecta interacts with the surrounding gas (circumstellar medium, CSM, or interstellar medium, ISM) creating a shock front at its outer edge. The CSM is the nearby surrounding gas affected by the progenitor star, whereas the ISM is more generally the large-scale gas between the stars. The general picture of SNR evolution is an initial ejecta-dominated (ED) stage, in which the effect of the ejected mass and explosion energy are both important. This evolves into a Sedov-Taylor (ST) phase, where only the explosion energy remains important because the mass swept up by the SN shock exceeds the ejected mass. For ED and ST phases, radiative energy losses by the hot shocked interior are negligible. As the SNR becomes older, radiative losses become more important until the post-shock pressure becomes significantly reduced. This causes formation of a dense cool shell just behind the shock front. However, the hot low density interior is unaffected by energy losses so the SNR is driven by the interior pressure acting on the dense shell. The SNR is then in the pressure driven snowplow (PDS) phase. During the entire evolution the outer shock front is slowing down with time. During the PDS phase, it can slow down enough that it is not distinguishable from random motions

in the ISM. This is the termination (or merger) of the SNR with the ISM. In some (rare) cases, the SNR can lose its interior pressure before merger, resulting in an additional phase, where the dense shell coasts outward, conserving momentum. This phase is called the momentum-conserving shell (MCS) stage.

The unshocked part of the ejected envelope has a homologous velocity profile ($v \propto r$ at fixed time). The outer edge interacts in the form of a shock structure with the CSM or ISM (hereafter, we use the term CSM, but whether the surrounding gas is CSM or ISM depends on the particular situation of the progenitor and distance of the shock from the SN). From outside to inside, this shock structure consists of: the undisturbed CSM, the outer shock moving into the CSM, a layer of shocked CSM, the contact discontinuity separating the shocked CSM from the shocked envelope, the layer of shocked envelope, the inner (or reverse) shock moving inward relative to the ejecta, and the undisturbed ejecta. After the reverse shock reaches the center of the SNR, the entire ejecta is fully shocked. Reflected shocks and sound waves are generated at this time, and die out over time (e.g. see CMB88). These are perturbations on the overall structure and are ignored in the models here (and the analytic models in CMB88 and TM99).

We assume that the structure is spherically symmetric so that it depends only on radius and time. The pre-shock external medium (CSM) is assumed to have constant density or a $1/r^2$ density profile centered on the SN. The latter is appropriate for a stellar wind with steady mass loss rate. Thus the CSM density is a power-law $\rho_{CSM} = \rho_s r^{-s}$, with $s=0$ (constant density medium) or $s=2$ (stellar wind density profile). The unshocked ejecta is taken to have a power-law density profile $\rho_{ej} \propto r^{-n}$.

With these assumptions the evolution of the forward and reverse shock has been calculated for the ED through ST phases (TM99). The early part of the ED phase follows a self-similar evolution, calculated by Chevalier (1982). We used the TM99 analytic solutions

for our modelling software, with some additional features as described below. There is no smooth transition from the $s=2$ ED and ST phases to the later radiative phases (e.g. TM99). Thus we consider the later phases only for the $s=0$ case. For the radiative phases we follow the treatment of CMB88, but modify their solutions to be consistent with the earlier ED to ST evolution.

We also consider some alternate models for SNR evolution which include additional physical effects. In particular, we include models for a SNR in cloudy ISM of White & Long (1991) (hereafter WL91), the constant energy loss model of Liang & Keilty (2000) (hereafter LK2000), and the model for SNR in hot ISM of Tang & Wang (2005) (hereafter TW2005).

3. Model calculations

3.1. General discussion

3.1.1. Mean molecular weights

The number density of electrons is n_e , of hydrogen nuclei is n_H , and of total number of ions is n_{ion} . Then the total mass density is given by $\rho = \mu_e n_e m_H = \mu_H n_H m_H = \mu_{ion} n_{ion} m_H = \mu_{tot} n_{tot} m_H$. Here μ_e is the mean mass per electron, μ_H is the mean mass per hydrogen nucleus, μ_{ion} is the mean mass per ion and μ_{tot} is the mean mass per particle (with $n_{tot} = n_e + n_{ion}$ is the total number of particles).

3.1.2. Characteristic time and radius scales

As discussed in TM99, non-radiative supernova remnants undergo a unified evolution. The characteristic radius and time, for SNR in a uniform ISM, are given by $R_{ch} = (M_{ej}/\rho_0)^{1/3}$

and $t_{ch} = E_0^{-1/2} M_{ej}^{5/6} \rho_0^{-1/3}$ with M_{ej} the ejected mass and E_0 the explosion energy. ρ_0 is the mass density of the ISM, $\rho_0 = \mu_H n_0 m_H$, where the ambient ISM hydrogen number density is n_0 . This gives characteristic velocity $V_{ch} = R_{ch}/t_{ch}$ and characteristic shock temperature $T_{ch} = \frac{3}{16} \mu_I \frac{m_H}{k_B} V_{ch}^2$. For SNR in a circumstellar medium with $\rho \propto r^{-s}$, $s=2$, the characteristic radius and time are given by $R_{ch} = (M_{ej}/\rho_s)$ and $t_{ch} = E_0^{-1/2} M_{ej}^{3/2} v_w / \dot{M}$, with \dot{M} and v_w the wind mass loss rate and velocity, and $\rho_s = \frac{\dot{M}}{4\pi v_w}$.

Radiative losses gradually become important (see CMB88 for details). The first parcel of SNR interior gas to cool completely defines the time of thin shell formation t_{sf} . Somewhat prior to t_{sf} , at t_{PDS} , cooling causes the postshock fluid velocity to approach the shock velocity and the pressure-driven-snowplow (PDS) phase begins. We use the standard cooling function $\Lambda = 1.6 \times 10^{-19} \zeta_m T^{-1/2} \text{ erg cm}^3 \text{ s}^{-1}$ with ζ_m the metallicity factor. This gives the same t_{sf} as in CMB88, i.e. $t_{sf} = 3.61 \times 10^4 E_{51}^{3/14} / (\zeta_m^{5/14} n_0^{4/7}) \text{ yr}$. Following CMB88, we define $t_{PDS} = t_{sf}/e$.

A SNR is considered to merge with the ISM when the shock speed is not significantly larger than the ambient thermal sound speed or larger than typical turbulent velocities in the ISM. The thermal sound speed is $c_{th} = \sqrt{\gamma k_B T_{ISM} / (\mu_H m_H)}$ with γ the adiabatic index, here taken as 5/3, and T_{ISM} the ambient ISM temperature. The turbulent velocity dispersion is taken as σ_v . Thus merger is defined when the SNR shock speed drops to $\beta \times c_{net}$ with $c_{net}^2 = c_{th}^2 + \sigma_v^2$ and β is a parameter which determines the limit for distinguishing the SNR shock from random speeds and is taken to be 2 here. In most cases a SNR will merge before it enters the momentum conserving shell stage (CMB88). In this case the timescale for merger is $t_{mrg} = 153 t_{PDS} [E_{51}^{1/14} n_0^{1/7} \zeta_m^{3/14} / (\beta c_6)]^{10/7}$ with $c_6 = c_{net} / (10^6 \text{ cm/s})$.

3.1.3. Electron-ion temperature equilibration

For the case of a gas consisting of a single species of particle with mass m , the post-shock temperature is $T_s = \frac{3m}{16k_B}V_s^2$. The post shock gas is a mixture of electrons and different species of ions. The shock wave heats the ions to a much higher temperature than the electrons because of the high ratio of ion to electron mass (~ 1800 for protons, higher for other ions). We follow the discussion of electron heating given in Cox & Anderson (1982), which uses the results of Itoh (1978). The electron-ion temperature equilibration timescale due to Coulomb collisions is: $t_{eq} = 5000E_{51}^{3/14}n_0^{-4/7}$ yr. The electron-to-ion temperature ratio is given by $g = T_e/T_{ion}$, with g given to a good approximation by

$$g = 1 - 0.97\exp[-(5f/3)^{0.4}(1 + 0.3(5f/3)^{0.6})]. \quad (1)$$

Here $f = \frac{\ln(\Lambda)}{81} \frac{4n_0}{T_s^{3/2}}(t - t_0)$ with the Coulomb logarithm given by $\ln(\Lambda) = \ln(1.2 \times 10^5 T_s^{1/2} T_e (4n_0)^{-1/2})$, t_0 is the time a parcel of gas was shocked and the post-shock density is $4n_0$. We approximate $t - t_0$ by $t/4$ here because the mean age of the shocked gas is $\sim t/4$. Observations show that young supernova remnants have a lower limit on T_e/T_{ion} of about 0.03 (see Fig. 2 of Ghavamian et al. (2013)). In the formula for g above we inserted the factor of 0.97, to obtain an early time limit of 0.03.

We apply the temperature ratio g to find both electron and ion temperatures from the shock velocity. For a single particle species one has $T_s/m = \frac{3}{16k_B}V_s^2$. For a mixture of species, electrons and ions, with mean mass per particle μ_e and μ_{ion} , respectively, one has

$$\frac{T_e}{\mu_e m_H} + \frac{T_{ion}}{\mu_{ion} m_H} = \frac{3}{16k_B}V_s^2. \quad (2)$$

This reduces to the correct result in the case of a single species. It also allows definition of the shock temperature, which is the temperature to which a (fictitious) species of mass $\mu_{tot}m_H$ would be heated, with $1/\mu_{tot} = 1/\mu_e + 1/\mu_{ion}$. With the electron to ion temperature ratio, g , and shock velocity V_s , one uses the above formulae to find T_e and T_{ion} .

3.1.4. Emission Measure and EM weighted temperature

The radiation from the hot shocked plasma in the interior of a SNR is dominated by two body processes, so it is proportional to the product of the electron and ion densities. (e.g. Raymond et al. (1976)). The emission measure, EM, is defined by the integral over volume of the product of electron density n_e and proton (or hydrogen ion) density n_H : $EM = \int n_e(r)n_H(r)dV$. EM depends on n_e , n_H and their dependence on radius in the interior of the SNR, and on the total volume of the interior, which depends on the shock radius, R_s . EM can be determined by analysis of X-ray spectrum observations of a SNR, so serves as a critical constraint on the state of the SNR. EM is given by the *norm* parameter from fitting the X-ray spectrum (see the XSPEC manual at heasarc.gsfc.nasa.gov):

$norm = \frac{10^{-14}}{4\pi D^2} EM$, with D , the distance to the SNR, and all units are assumed to be cgs. An estimate of the magnitude of EM can be done using a uniform SNR interior with typical parameters $n_e = n_H = 1 \text{ cm}^{-3}$, $R_s = 5\text{pc}$ to obtain $7.7 \times 10^{58} \text{cm}^{-3}$. Thus EM is often expressed in units of 10^{58}cm^{-3} .

To calculate EM from a SNR model, the interior density profile of the SNR is required. During the self-similar phases of evolution of a SNR, the shape of the profile is constant with only the overall normalization and scaling with radius changing with time. Thus we define the dimensionless EM, dEM , by

$$dEM = EM / (n_{e,s} n_{H,s} R_s^3) \quad (3)$$

with $n_{e,s}$ and $n_{H,s}$ the values of n_e and n_H immediately inside the shock front. dEM is independent of time for the self similar phases of evolution. Here the shock is assumed to be a strong shock with compression ratio of 4, so that $n_{H,s}=4n_H$ with n_H the ISM value. $n_{e,s}$ is determined by $n_{H,s}$ and the mean molecular weights of the post-shock gas.

The observed temperature of a SNR, derived from the X-ray spectrum, depends on

the state of the SNR and on the X-ray spectrum model used. For most SNRs, a single electron-temperature non-equilibrium ionization model is used. In this case, the observed temperature measures the emission weighted temperature of the emitting gas. We define the dimensionless temperature dT by:

$$dT = \frac{1}{T_s} \frac{1}{EM} \int n_e(r)n_H(r)T(r)dV \quad (4)$$

i.e., the emission weighted temperature is $dT \times T_s$. For the self-similar phases of evolution of an SNR, the temperature structure has a constant shape, normalized by the temperature at the shock front, so that dT is a constant.

3.1.5. Surface brightness profile and luminosity

The surface brightness of a SNR depends on the line-of-sight integral of the emission coefficient, given by: $I(b, \nu) = \int j(\nu)ds$, where the integral is taken along the line of sight through the SNR at impact parameter b from the SNR center. The volume emission coefficient $j(\nu)$ is given in terms of the emissivity $\epsilon(\nu)$ by $j(\nu) = n_e n_H \epsilon(\nu)$. In general $\epsilon(\nu)$ depends on the history of the particular parcel of emitting gas, but usually this is simplified. For example $\epsilon(\nu)$ can be taken as depending only on current temperature, $T(r)$ of the parcel. For simplicity, we use this approximation here. A better approximation is that it depends on temperature and on an ionization timescale parameter $n_H t$ or, equivalently, on an ionization parameter $\eta = n_H^2 E$ (Hamilton et al. (1983), Borkowski et al. (2001)).

For simplicity, here we calculate the surface brightness profile using thermal bremsstrahlung as the emission mechanism. This is only a rough approximation of the emission from an ionized plasma (e.g. see Raymond et al. (1976) and Hamilton et al. (1983)). The bremsstrahlung emission coefficient, in units of $\text{erg s}^{-1}\text{cm}^{-3} \text{Hz}^{-1}\text{sr}^{-1}$, is

$$j_B(x, dE) = 5.4 \times 10^{-39} (Z^2)_{av} n_e(x) n_{ion}(x) T_s^{-1/2} T_d(x)^{-1/2} ga(x, dE) \exp(-dE/T_d(x)). \quad (5)$$

Here $x = r/R_s$ is radius scaled by the shock radius, $T_d(x) = T(x)/T_s$ is interior temperature scaled by the shock temperature and $dE = h\nu/(k_B T_s)$ is the photon energy divided by $k_B T_s$. Thus the argument of the exponential reduces to $h\nu/(k_B T(x))$. ga is the Gaunt factor and $(Z^2)_{av}$ is the mean value of Z^2 for the plasma. $n_e(x)$ and $n_{ion}(x)$ are given by the interior density profile of the SNR, normalized to 1 at the shock front, times the values at the shock front $n_{e,s}$ or $n_{ion,s}$. Thus we obtain the surface brightness at a given scaled photon energy dE :

$$I(b, dE) = \int j_B(x(s), dE) ds \quad (6)$$

where $x(s) = \sqrt{b^2 + s^2}/R_s$ is the scaled radius along the line of sight at a given impact parameter b . The total luminosity of the SNR at a given scaled photon energy dE is given by integrating the surface brightness over the area of the SNR, which is equivalent to integrating the emission coefficient over volume of the SNR: $L_\nu(dE) = \int_0^{R_s} I(b, dE) 2\pi b db$. The luminosity in any given energy band E_1 to E_2 is obtained by integrating L_ν over the scaled energy range $dE_1 = E_1/(k_B T_s)$ to $dE_2 = E_2/(k_B T_s)$.

3.2. Standard evolutionary path

3.2.1. Ejecta Dominated (ED) and Sedov-Taylor (ST) stages

The ED phase is the time during which the ejected mass dominates over the swept-up mass from the CSM on the evolution of the SNR. The ST phase is the time after the effects of ejected mass are dominant but prior to onset of radiative losses. We refer to the so-called standard ST solution, which assumes zero ejected mass, as "pure ST" to differentiate it from the ST phases calculated by TM99, which include the effects of non-zero ejected mass.

The evolution starts with the early ED self-similar phase, previously considered by Chevalier (1982) for $n > 5$. The shock evolution during the full ED and ST phases can

be calculated using the results of TM99. They consider the full non-radiative evolution of a SNR, which ends with the start of transition to the PDS radiative phase at time t_{pds} . During the ED phase, the reverse shock propagates inward into the ejecta, eventually reaching the center of the SNR. A core-envelope structure for the ejecta is assumed with constant density core and power-law density envelope, with index n . For $n < 3$, the core can be taken to have zero size. For $n > 5$ the outermost velocity of the envelope v_{ej} does not affect the mass or energy of the envelope so that the parameter v_{core}/v_{ej} can be taken to be zero (by taking the limit $v_{ej} = \infty$). Here we calculate SNR forward and reverse shock evolution for uniform CSM ($s=0$) for the following cases of ejecta power law index: $n=0, 2, 4, 6, 7, 8, 9, 10, 12$ and 14 . For the CSM wind profile case ($s=2$), we calculate $n=0, 1, 2$ and 7 cases.

First consider the $s=0$ cases. For $n=0$ we use the solutions given in Table 5 of TM99. For this case the reverse shock reaches maximum radius at $1.046t_{ch}$. The early self-similar evolution, with constant ratio of reverse shock radius R_r to forward shock radius R_b , ends much earlier: it is violated at the 5% level by $0.175t_{ch}$. For $n=2$, we use the solutions of TM99 with parameters given in their Table 3, noting that their Table 4 solutions contain some incorrect numbers, inconsistent with Table 3. For $t < t_{ST}$, the solutions are specified by $t(R_b)$ and $t(R_r)$, so these are inverted using a root finding algorithm to yield $R_b(t)$ and $R_r(t)$, hence $V_b(t)$ and $V_r(t)$. For $n=4$ and $t < t_{ST}$, we use the TM99 equations (47), (48) and (49). For $n=4$ and $t > t_{ST}$, we use the TM99 equations (57) and (58). However to better match their $n=4$ numerical solutions for the reverse shock given in their Figs. 4 and 5, we add an acceleration term to $R_r(t)$ for $t > t_{core}$. As for $n=2$, for $t < t_{ST}$ the relations $t(R_b)$ and $t(R_r)$ are inverted to get the solutions. For $n=6, 7, 8, 9, 10, 12$ and 14 , we use the $n > 5$ solutions of TM99. For $R_b(t)$, the solution is specified by their equations (75) and (76) for $t < t_{ST}$ and equations (57), (81) and (82) for $t > t_{ST}$. For $R_r(t)$, the solution is specified by their equation (77) and $R_r = R_b/l_{ED}$ for $t < t_{core}$ and equations (83) and (84)

for $t > t_{core}$ until the reverse shock hits the center.

Next we discuss the $s=2$ cases. For $n= 0, 1$ and 2 we use the solutions from Table 8 of TM99 and invert $t(R_b)$ to get $R_b(t)$ then use $R_r = R_b/l_{ED}$. For $n= 7$ we use the solutions from Table 9 of TM99, which is the same as that from Chevalier (1982).

3.2.2. Pressure-driven snowplow (PDS) phase, momentum-conserving shell (MCS) phase and merger

We follow the treatment given in CMB88 for the radiative phases for SNR in a uniform CSM ($s=0$ case). The different cases above with different ejecta profiles (values of n) have radii different at a given time than the pure Sedov-Taylor solution (see Results section). Thus the matching of radiative phases onto the non-radiative phase has to be done differently than in CMB88. CMB88 investigated numerical hydrodynamic solutions of SNR evolution, then compared those to analytic models for blast wave evolution. They then fit an offset power-law as a good approximation to the numerical solutions. However this creates a discontinuity in velocity at t_{pds} where the relation $V_b = dR_b/dt$ is violated. In order to get a smooth evolution of the blast wave radius and velocity and also satisfy $V_b = dR_b/dt$ at all times, we include a smooth transition. We linearly interpolate the shock velocity from the value at t_{pds} from the previous phase to the value in the PDS phase at time $1.1t_{pds}$. Then we integrate the equation $V_b = dR_b/dt$ to get $R_b(t)$ at all times for $t > t_{pds}$.

To determine when the PDS phase ends we calculate the merger time t_{mrg} and the onset of the MCS phase t_{mcs} , as defined in CMB88. If $t_{mrg} < t_{mcs}$ then the evolution is terminated. If $t_{mrg} > t_{mcs}$ then V_b for the MCS phase is calculated similarly to that for the beginning of the PDS phase, by interpolating between t_{mcs} and $1.1t_{mcs}$ and then integrating

$$V_b = dR_b/dt.$$

3.3. Alternate SNR evolution models

3.3.1. SNR in cloudy ISM

We follow the treatment of WL91, which presented self-similar models for SNR evolution in a cloudy ISM. The self-similar models are similar to the standard self-similar Sedov-Taylor model for the evolution of the blast wave radius, although the interior structure of the cloudy SNR models is drastically different. The WL models depend on two parameters: a cloud density parameter $C = \rho_c/\rho_0$, with ρ_c is the ISM density if the clouds were uniformly dispersed in the ISM; and an evaporation timescale parameter $\tau = t_{evap}/t$, with t_{evap} the evaporation timescale and t the age of the SNR. The WL models reduce to a one parameter set which depend on C/τ , in the limit τ approaches ∞ . We use these one parameter models, in particular, the three cases $C/\tau=1, 2$ and 4 . The WL91 model is strictly applicable, like the standard Sedov-Taylor model, for the case of zero ejected mass, and evolution in a cloudy ISM from $t=0$. We join the cloudy SNR models onto the earlier phases with finite ejected mass at time t_{ST} . Earlier than t_{ST} , the SNR blast wave evolution is dominated by the interaction of the ejecta, so the effects of a cloudy ISM are hard to determine and have not yet been investigated in enough detail. The transition to cloudy SNR evolution is calculated by interpolating the forward shock velocity V_b at t_{ST} , to the velocity given by the WL91 model at $1.1t_{ST}$. Then R_b is found by integrating $V_b = dR_b/dt$ for $t > t_{ST}$.

The cloudy SNR phase ends when radiative cooling becomes important. However it ends very differently than for the ST phases described above. Rather than entering a PDS phase, the SNR enters directly into the MCS phase. This happens because of the interior

structure for the WL91 models (see Fig.2 of WL91). Because the temperature and density are much more uniform than for the ST models (pure ST model and ST models of TM99), the whole interior of the cloudy SNR cools at nearly the same time, which results in the loss of interior pressure at nearly the same time that the forward shock evolution is affected by loss of pressure.

3.3.2. Fractional energy loss model

LK2000 introduced an analytic model for radiative blast wave evolution, based on the thin shell approximation. They introduced a parameter γ_1 which determines the fractional energy loss rate at the shock front, ϵ by the relation: $\epsilon = 4 \frac{\gamma - \gamma_1}{\gamma - 1} (\gamma_1 + 1)^{-2}$. Here γ is the adiabatic index of the gas (both upstream and downstream) and γ_1 is constrained by $1 \leq \gamma_1 \leq \gamma$. The post-shock expressions for pressure, velocity and density are the conventional expressions but with γ replaced by γ_1 (see LK2000). The total energy content of the blast wave decreases with time as a result of the energy loss: $dE/dt = -2\pi\rho_0 V_b^3 R_b^2 \epsilon$. The momentum conservation equation, with internal driving pressure, determines the motion of the blast wave: $dV_b/dR_b = 3(\alpha - 1)V_b/R_b$, with the ratio of interior pressure p_c to post-shock pressure p_f given by $\alpha = p_c/p_f$. The total energy of the SNR is given by the kinetic energy of the shell plus the internal energy of the hot interior (equation 6 of LK2000). Then α is given by $\alpha = (2 - \gamma + [(2 - \gamma)^2 + 4(\gamma_1 - 1)]^{1/2})/4$. As in LK2000 we define $n_\alpha = 1/(4 - 3\alpha)$, then integrate the equation of motion for V_b . However we use different boundary conditions than LK2000 so obtain different solutions for $R_b(t)$ and $V_b(t)$. I.e. we join the constant energy loss solution onto an earlier phase of SNR evolution at time t_0 , with radius R_0 and velocity V_0 . The resulting solution is:

$$R_b(t) = [R_0^{1/n_\alpha} + (4 - 3\alpha)R_0^{3-3\alpha}V_0(t - t_0)]^{n_\alpha} \quad (7)$$

and

$$V_b(t) = V_0[R_b(t)/R_0]^{3\alpha-3}. \quad (8)$$

The above solution was derived using the momentum equation for a thin shell. However, when one sets $\epsilon = 0$ and uses initial t_0 , R_0 and V_0 from the pure ST stage, one recovers the pure ST evolution for $R_b(t)$ and $V_b(t)$. The evolution of $R_b(t)$ and $V_b(t)$ for the constant energy loss model with $\epsilon = 0$ also reduces to the TM99 evolution for the various n values in the ST phase. When choosing a non-zero fractional energy loss $\epsilon > 0$, the shock front decelerates more rapidly than for the respective adiabatic phases (pure ST phase or TM99 ST phases). This is expected because of the reduced post-shock pressure resulting from the energy loss. In our SNR modelling software, we allow the user to have fractional energy loss phase start at any time in the ST or PDS phases. Prior to t_{ST} , the fractional energy loss model does not properly represent the SNR evolution.

3.3.3. SNR in hot low-density medium

The evolution of a SNR in a hot low-density medium deviates significantly from the ST evolution because of the effects of swept-up energy from the ISM and of the high sound speed Tang & Wang (2005)(hereafter TW2005). They verified their analytic approximations with hydrodynamic simulations. The effects of a hot ISM are large for the evolution if the critical time t_c is less than the shell formation timescale for the SNR, t_{sf} . t_c is defined by $t_c = [(2\zeta_1/5)^5 E_0 / (\rho_0 c_{th}^5)]^{1/3}$ with $\zeta_1 = 2.026^{1/5}$ (see TW2005). If $t_c < t_{sf}$, then the SNR never enters the radiative phase but instead has an outer velocity which asymptotically approaches the sound speed in the hot ISM.

Instead of matching the hot-ISM SNR solution onto a pure ST model (as done in TW2005), we match to any of the TM99 ST phases at time t_M , which has a default value

of $0.1t_c$. At earlier times than $\simeq 0.1t_c$, the analytic solution is not a good match to the hydrodynamic solutions (see TW2005 Fig.1). This gives the following evolution for SNR outer velocity:

$$V_H(t) = c_{th}[t_H/t + 1]^{3/5} \quad (9)$$

with $t_H = [(V_b(t_M)/c_{th})^{5/3} - 1]t_M$. The SNR outer radius is found by integration of the velocity:

$$R_H(t) = R_M + \int_{t_M}^t V_H(t)dt. \quad (10)$$

3.4. Implementation notes

The models were originally programmed in MathCad and then programmed in Python. For debugging and verification of the calculations, the results from both codes were compared for a extensive of cases.

The input parameters for the SNR model calculations are as follows. The SNR explosion parameters are: age (in yr), energy E_0 (units 10^{51} erg), ejected mass M_{ej} (units M_\odot), ejecta power-law index n . The ambient medium parameters are: power-law index s (0 or 2), temperature T_{ISM} , cooling adjustment factor ζ_m (1 for solar abundance) and ISM turbulence or random speeds σ_v (km/s). For $s=0$, density is specified by ISM number density. For $s=2$, input parameters are wind mass loss rate (M_\odot /yr) and wind speed (km/s). The electron to ion temperature ratio is calculated as described above, but alternately can be entered by hand.

Element abundances for the ISM or CSM and for the ejecta are specified by user input. For simplicity, in the program we include the elements H, He, C, N, O, Ne, Mg, Si, S and Fe, which are the ten most abundant elements in Solar abundances. The abundances are specified in standard form, i.e. by $\log(X/H) + 12$ with X/H is the number of nuclei of

element X divided by the number of H nuclei. The default values for the ISM abundances are solar values, taken from Grevesse & Sauval (1998), or LMC values, taken from Russell & Dopita (1992). For ejecta abundances, default values were taken (in units of $\log(X/H) + 12$) as follows: for core-collapse SN- He: 11.22, C: 9.25, N: 8.62, O: 9.69, Ne: 8.92, Mg: 8.30, Si: 8.79, S: 8.54, Fe: 8.55; for Type Ia SN- He: 11.40, C: 12.60, N: 7.50, O: 12.91, Ne: 11.04, Mg: 11.55, Si: 12.75, S: 12.43, Fe: 13.12. The pop-up window that specifies abundances allows individual abundances for the 9 elements relative to H to be specified by the user.

Additional inputs for the alternate models, which all require $s=0$, are as follows. For the cloudy ISM model, the input is C/τ (1, 2, or 4). For the fractional energy loss model, inputs are adiabatic index γ , fractional energy loss ϵ , and model start time (within ST or PDS phases). For the hot low-density ISM model (available if $0.1t_c < t_{pds}$) the input is the end time.

Outputs from the program are as follows. Plots are produced for R_b and R_r (if applicable) vs. time, and for V_b and V_r (if applicable) vs. time. Values are given, at the specified age, for blast-wave shock temperature for electrons, reverse shock temperature for electrons, blast-wave radius and velocity, reverse shock radius and velocity. Also given are the transition times between ED and ST phases, between ST and PDS phases, between PDS and MCS phases (if applicable), and merger time. Emissivity related values and luminosity are calculated only for phases for which the internal structure (density and temperature) are determined by self-similar models. Those phases are: the ED phase for $t < t_{core}$ (see TM99); the ST phase for $t > t_{rev}$ where t_{rev} is the time that the reverse shock hits the center of the SNR; and the cloudy ISM models (see WL91). As noted in Section 3.1.4 above, for the self-similar phases the dimensionless emission measure and dimensionless temperature are constant with time. These values (dEM and dT) were calculated using the self-similar interior solutions for density and temperature and given in Table 1 below. For

the ED phase, the values for the forward and reverse shocked material are given for the two cases $s=0, n=7$ and $s=0, n=12$.

4. Results and Discussion

The model calculations were tested by verifying results in TM99, CMB88, WL91, LK2000 and TW2005. The MathCad version of the program and Python version were compared for verification. The MathCad version was recently used to model the set of 50 SNRs for which good observations were available, and to derive properties of this set of SNRs (Leahy (2016)). To illustrate the SNR evolution modelling software, we present the following cases.

The main window of the program takes input parameters required to specify the SNR evolution, see Fig. 1. ISM and ejecta abundances can be selected in a pop-up menu from standard abundance sets or else the element abundances can be specified individually. The model type can be selected from the models described above: either the standard SNR evolution, fractional energy loss model, cloudy ISM model or Hot low-density ISM model. The main window produces several outputs. These include a plot of shock radius or velocity vs. time; shock radius, velocity and electron temperature for the specified input age; and the phase transition times.

For the ED and early ST phases, we compare calculations of forward (or blastwave) and reverse shock radii, R_b and R_r , in Fig. 2. Cases with $s=0$ and $n=0, 2, 4, 7, 10$ or 14 are shown. Input parameters of $E_0 = 10^{51}$ erg, $M_{ej} = 1.0 M_\odot$, $n_0 = 2 \text{ cm}^{-3}$, $T_{ISM} = 100$ K, $\zeta_m = 1$ and $\sigma_v = 7 \text{ km/s}$ were used. The forward shock radius is largest for $n=4$ and smallest for $n=7$ (see also Fig. 4 below). The reverse shock lifetime is longest for the $n=2$ case, but reaches the largest radius for the $n=14$ case.

The Emissivity button on the main screen of the program brings up calculation of various quantities calculated from the interior structure of the SNR. Sample results for the ED phase are shown by the screenshot in Fig. 3, for the case $s=0$, $n=7$. We use ejecta composition typical for core collapse SN and solar abundances for the ISM. Emission measures are given for the forward shocked material, between the forward shock and the contact discontinuity, and for the reverse shocked material, between the reverse shock and the contact discontinuity. For this case the forward shock EM is larger by a factor of 1.9. In general, the emission weighted temperature is different than the temperature at the shock front. This is caused by the temperature and density profiles behind the shock front. In this case, the electron temperature at the forward shock front is $9.3 \times 10^7 \text{K}$ compared to the emission weighted temperature of $11.4 \times 10^7 \text{K}$. For the reverse shock the electron temperature at the reverse shock is $4.1 \times 10^7 \text{K}$ whereas the emission weighted temperature of reverse shocked material is $5.9 \times 10^7 \text{K}$. Radial profiles of temperature and density are given as a function of r/R_s . The surface brightness profile $I(b, E)$, using the bremsstrahlung emissivity as described above, is given for a user specified photon energy, E , in keV. The SNR spectrum L_ν is calculated by integrating $I(b, E)$ over the face of the SNR for a given input energy range, and the total luminosity L over the same energy range is calculated. The luminosity from the forward shocked material and reverse shocked material are calculated separately.

Next we consider the ST phase and compare the shock radii and velocities for different ejecta profiles, n , and with the pure ST model. We find that there is a significant difference between pure ST and ST evolution for different ejecta profiles n . The left panel of Fig. 4 shows blast wave radius, calculated with the input parameters above. We note that pure ST is equivalent to setting the ejecta mass equal to zero. Both the ejected mass and how it is distributed affect the evolution of R_b : the different cases of ejecta power-law index, n , differ by similar amounts to the difference with pure ST. For $n=7$, the forward shock radius

R_b is smaller than for pure ST by 8%, 3.7% and 0.8% at t_{ch} , $2t_{ch}$ and $10t_{ch}$, respectively. The % difference decreases with time, although absolute difference is nearly constant in time. The shock velocities V_b differ by even more with differences of 13%, 6% and 1.1% for the same three times. The outer shock radius (R_b) evolution for $n=10$ to 14 is nearly identical (see Fig. 2 right panel). Thus these cases differ the most from pure ST (Fig. 4 left panel). If one uses a pure ST model and uses radius as an age proxy, the SNR age will be underestimated compare to the more accurate $n=7$ to $n=14$ models. The age error is significant, at about 15%. The velocities for the various cases are compared in the right panel of Fig. 4. It is seen the ST evolution for various n has larger velocity at a given time than pure ST. If one uses velocity as an age proxy, the SNR age will be underestimated using pure ST compared to the more accurate $n=7$ to $n=14$ models, similar to the case for using radius as an age proxy.

An example of outputs of the Emissivity calculation for the ST phase is shown by the screenshot in Fig. 5, for the case $s=0$, $n=7$. Emission measure and emission weighted temperature are calculated. The electron temperature at the forward shock front is 2.37×10^7 K compared to the emission weighted temperature of 3.05×10^7 K. Radial profiles of temperature and density are given as a function of r/R_s . The surface brightness profile $I(b, E)$, using the bremsstrahlung emissivity, is given for the input specified energy, in this case 1 keV. The SNR spectrum L_ν is calculated over the input energy range of 0.3 to 8 keV, and the total luminosity L over the same energy range is calculated.

The late-time SNR evolution is illustrated in Fig. 6. In this case to obtain the MCS phase to occur prior to merger, the parameters were taken as $E_0 = 10^{50}$ erg, $M_{ej} = 1.0 M_\odot$, $n_0 = 0.1 \text{ cm}^{-3}$, $T_{ISM} = 30$ K, $\zeta_m = 2$ and $\sigma_v = 0.3$ km/s. The left panel shows shock radius $R_b(t)$ for the ST phase $n=0$ case (labelled $R_{b,0}$), for the PDS solution joined to ST $n=0$ solution (labelled R_{pds}), for the full joined solution (labelled R_{mcs}). The latter includes

ST, PDS and MCS evolution. The decrease of shock speed at the ST to PDS transition (at $\sim 2.4 \times 10^4$ yr) and decrease at the PDS to MCS transition (at $\sim 10^7$ yr) are clearly seen. In the right panel, the deceleration parameter $m = V_b t / R_b$ is shown for the full joined solution (ST to PDS to MCS). During the ST to PDS evolution (between 10^4 to 10^5 yr), m drops from the pure ST value of 0.4 to $\simeq 0.3$ for the PDS phase. At the end of the PDS phase there is a rapid drop to a value of $\simeq 0.16$ followed by a slow increase. The behaviour of a gradual drop of m from 0.4 to 0.3 for the ST to PDS transition was found by CMB88 (their Fig. 5). They also note that practically (i.e. for most cases of realistic input parameters) the MCS stage does not occur. This is in agreement with the current calculations: to obtain an MCS stage we had to use a small explosion energy and low ISM density, and we also had to use a cold ($T_{ISM} < 40\text{K}$) and very quiet ($\sigma_v < 1$ km/s) ISM. The latter two restrictions are unrealistic for a low density ISM, confirming that the MCS phase can occur only in rare circumstances.

We illustrate the effect of evolution of a SNR in a cloudy medium next. In the left panel of Fig. 7, shock radii for the pure ST model, the ST n=0 model and cloudy SNR models are compared. The cloudy SNR models are calculated for $C/\tau = 1, 2$ and 4. These cloudy SNR models are all joined at small t onto the ST n=0 model. The radius of the cloudy SNR is much smaller than pure ST (by 8% for $C/\tau = 1$, up to 20% for $C/\tau = 4$, with the difference nearly constant in time). The difference between the cloudy models and the ST n=0 model is similar. In the right panel of Fig. 7 the corresponding shock velocities of the different models are compared. This shows that the shock velocities are lower for the cloudy models (by $\sim 10\%$ to 20%) than the pure ST model or ST n=0 model.

The evolution of a SNR occurring in a hot ISM is illustrated in Fig. 8. The input parameters for this case are: $E_0 = 10^{51}$ erg, $M_{ej} = 1.0 M_\odot$, $n_0 = 1 \text{ cm}^{-3}$, $T_{ISM} = 10^6$ K, $\zeta_m = 0.1$ and $\sigma_v = 7$ km/s. The left panel of Fig. 8 shows the evolution of blast-wave

radius for the case of the standard evolution, without including the effect of swept-up ISM thermal energy for the ST phase, $R_{b,ST}$, followed by the PDS phase, R_{PDS} , and ending with merger. Recall that time of merger with the ISM was defined as the time that shock velocity drops to $\beta \times c_{net}$ where net speed of sound c_{net} includes thermal and random motions, and β was taken as 2. The left panel also shows shock radius for the hot ISM model, R_H . It lasts significantly longer. The right panel of Fig. 8 shows the shock velocities for the standard model ($V_{b,ST}$ and V_{PDS}) and for the hot ISM model (V_H). The deceleration of velocity is much slower for the hot ISM model, after about 1.5×10^4 yr. This results in the velocity reaching the merger velocity at much later time. For a slightly cooler ISM, $T_{ISM} = 0.5 \times 10^6$ K, the swept up energy of the ISM is not enough to prevent the standard evolution from taking place (PDS and merger occurs before the shock velocity is affected significantly).

5. Summary and Conclusion

The different evolutionary phases for spherically symmetric SNR evolution have been described by analytical solutions. The phases include the full evolution, from the early ejecta-dominated stage to the merger with the interstellar medium. Joining of the different phases of evolution has been done in a consistent way, so that a continuous evolution in shock radius and velocity is obtained for the whole SNR evolution. In addition to the standard, optional evolutionary models have been described, including evolution in a cloudy ISM, the fractional energy loss model, and evolution in a hot low-density ISM.

These analytic descriptions have been incorporated into a Python code which has a graphical interface. The interface takes the SN explosion parameters and the CSM/ISM parameters as inputs and produces a number of outputs. The outputs include plots of shock radius and velocity vs. time, transition times between evolutionary phases and other

useful information. It also includes the SNR surface brightness profile at a specified photon energy, the SNR integrated spectrum and luminosity.

The program has been used here to illustrate some properties of SNR evolution, such as the significant difference between shock radius and velocity between pure Sedov-Taylor evolution and more realistic models which include the effects of ejected mass. This software is intended for two purposes: for understanding SNR evolution; and for modelling SNR observations to determine good estimates of SN explosion properties, SNR evolutionary state and ISM properties. The program is available in two forms, as Python code or as a windows executable. It can be obtained from GitHub (repository [denisleahy/SNRmodels](https://github.com/denisleahy/SNRmodels)) or from www.quarknova.ca (under software). The README.txt file has installation instructions. Those who use the software are requested to reference the current publication in any published work.

This work was supported by a grant from the Natural Sciences and Engineering Research Council of Canada.

REFERENCES

- Borkowski, K. J., Lyerly, W. J., & Reynolds, S. P. 2001, *ApJ*, 548, 820
- Chevalier, R. A. 1982, *ApJ*, 258, 790
- Cioffi, D. F., McKee, C. F., & Bertschinger, E. 1988, *ApJ*, 334, 252
- Cox, D. P., & Anderson, P. R. 1982, *ApJ*, 253, 268
- Ghavamian, P., Schwartz, S. J., Mitchell, J., Masters, A., & Laming, J. M. 2013, *Space Sci. Rev.*, 178, 633
- Grevesse, N., & Sauval, A. J. 1998, *Space Sci. Rev.*, 85, 161
- Hamilton, A. J. S., Sarazin, C. L., & Chevalier, R. A. 1983, *ApJS*, 51, 115
- Itoh, H. 1978, *PASJ*, 30, 489
- Itoh, N., Kawana, Y., & Nozawa, S. 2002, *Nuovo Cimento B Serie*, 117, 359
- Leahy, D. A. 2016, [arXiv:1612.00468](https://arxiv.org/abs/1612.00468)
- Liang, E., & Keilty, K. 2000, *ApJ*, 533, 890
- Raymond, J. C., Cox, D. P., & Smith, B. W. 1976, *ApJ*, 204, 290
- Russell, S. C., & Dopita, M. A. 1992, *ApJ*, 384, 508
- Tang, S., & Wang, Q. D. 2005, *ApJ*, 628, 205
- Truelove, J. K., & McKee, C. F. 1999, *ApJS*, 120, 299
- Vink, J. 2012, *A&A Rev.*, 20, 49
- White, R. L., & Long, K. S. 1991, *ApJ*, 373, 543

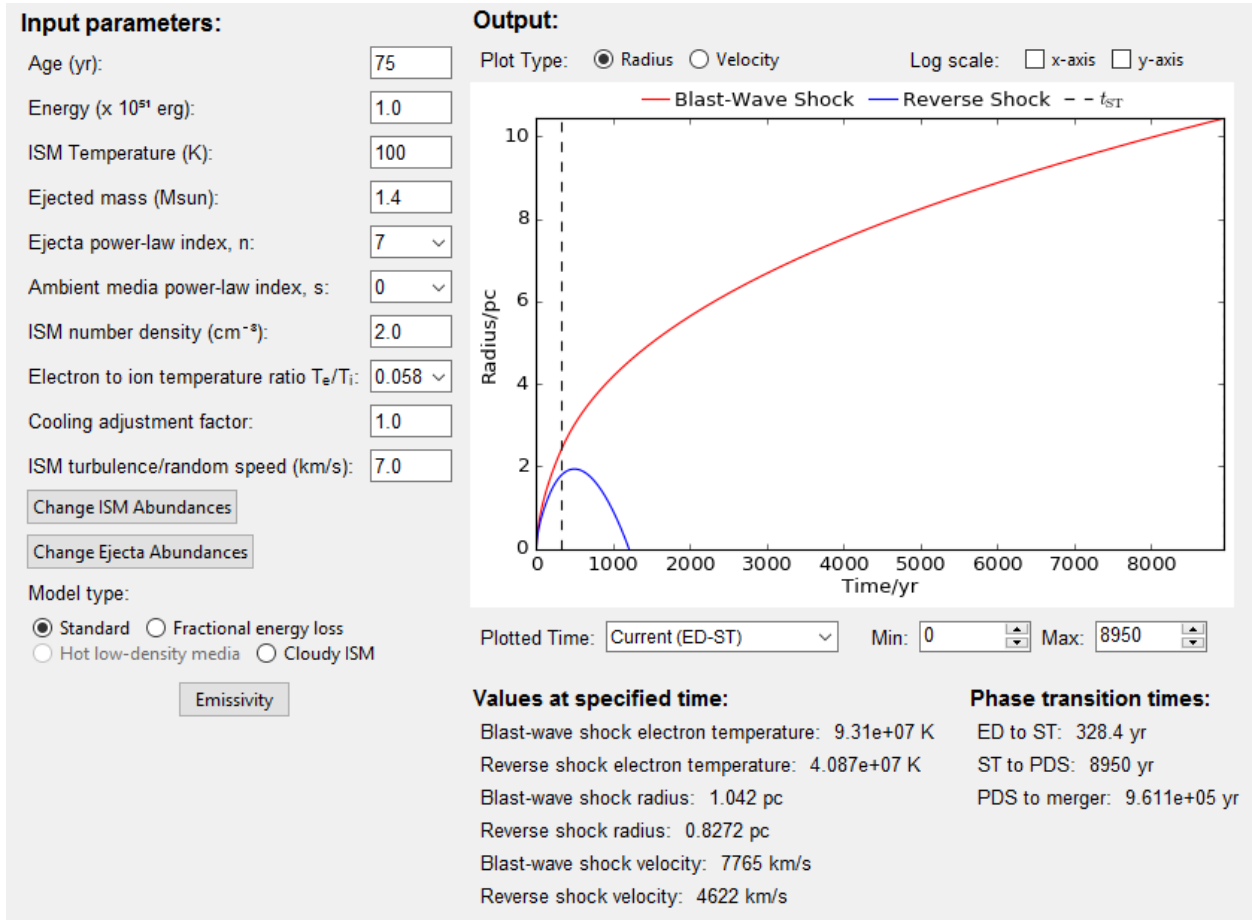


Fig. 1.— Screenshot of the main screen of the SNR modelling program. Left hand side: input parameters (boxes). Buttons specify the model type or bring up windows for entering ISM and ejecta abundances. Upper right: output plot of radius or velocity vs. time. Lower right: output values at the specified time and the phase transition times. Lower left: the Emissivity button brings up the calculation of emissivity and luminosity.

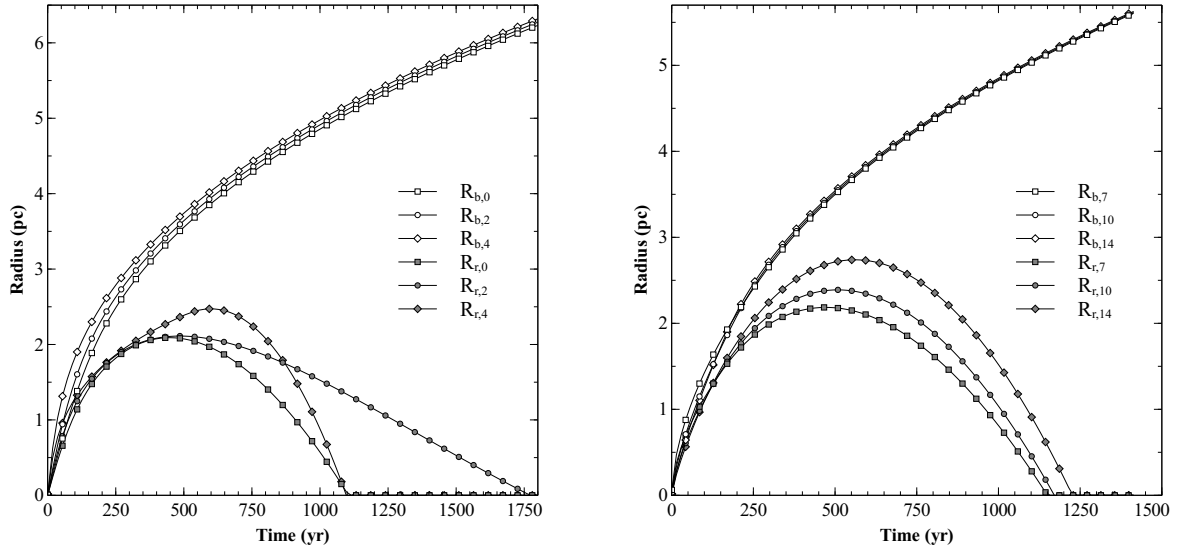


Fig. 2.— The time evolution of blast-wave radius (R_b) and reverse shock radius (R_r) vs. time: for ejecta density profiles with $n=0, 2$ and 4 (left panel) and for for ejecta density profiles with $n=7, 10$ and 14 (right panel).

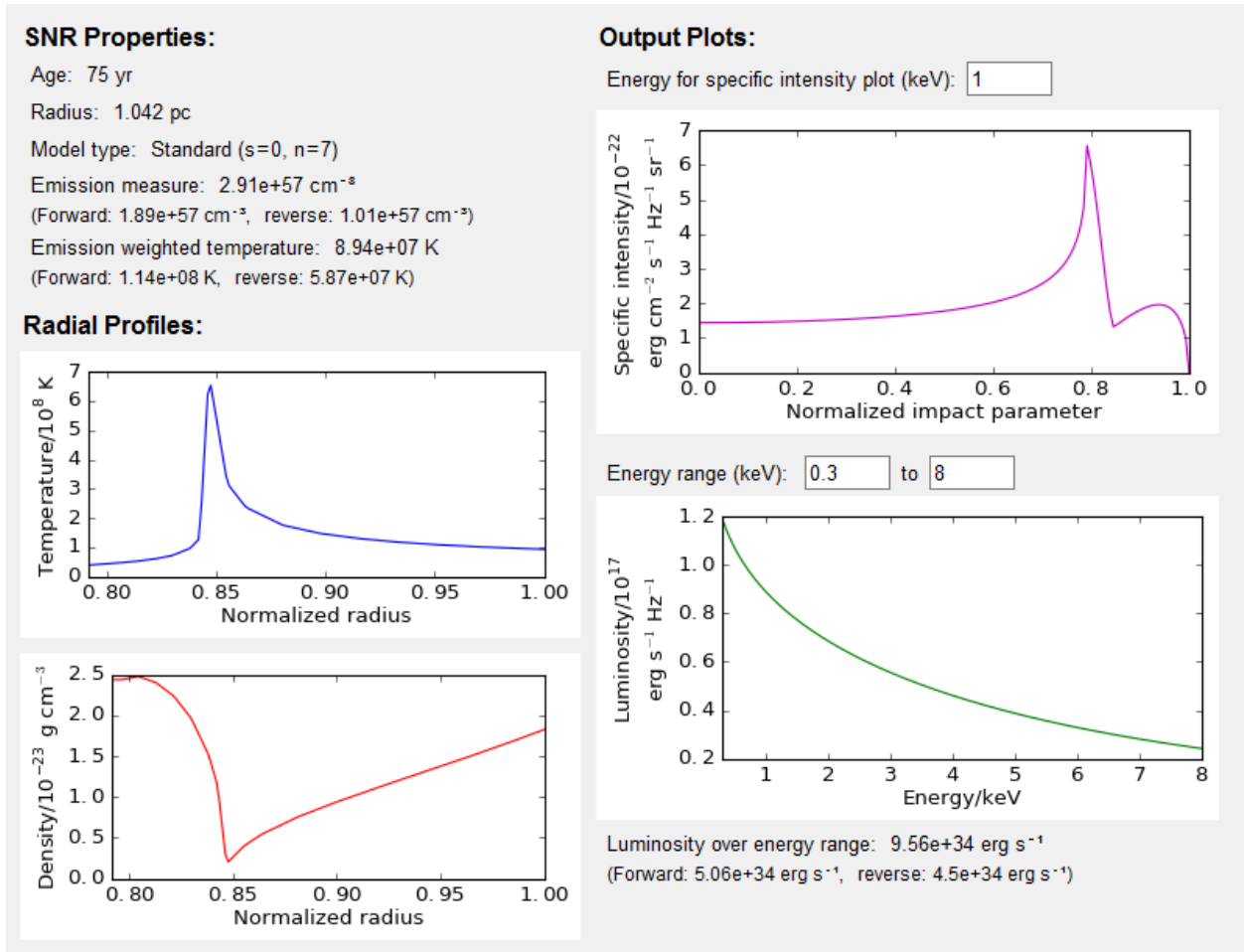


Fig. 3.— Screenshot of the Emissivity calculation tool of the SNR modelling program: For a SNR in the ED phase at age 75 yr with ejecta power law index $n=7$ in a uniform CSM ($s=0$): radial profile of temperature (top left) and of density (bottom left). Surface brightness profile at 1 keV (top right panel) and spectrum integrated over the volume of the SNR (bottom right panel).

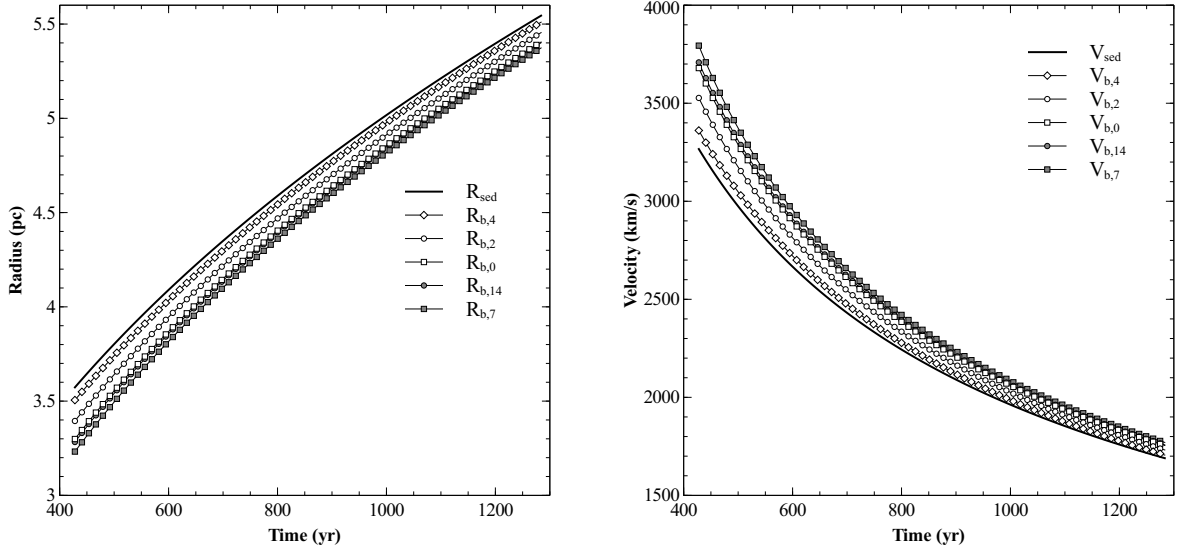


Fig. 4.— The time evolution of blast-wave radius (R_b) and velocity V_b vs. time. Left panel: comparison of pure Sedov-Taylor solution R_{sed} with R_b for ejecta density profiles with $n=0, 2, 4, 7, 10$ and 14 . Right panel: comparison of shock velocities: pure Sedov-Taylor solution V_{sed} with V_b for ejecta density profiles with $n=0, 2, 4, 7, 10$ and 14 .

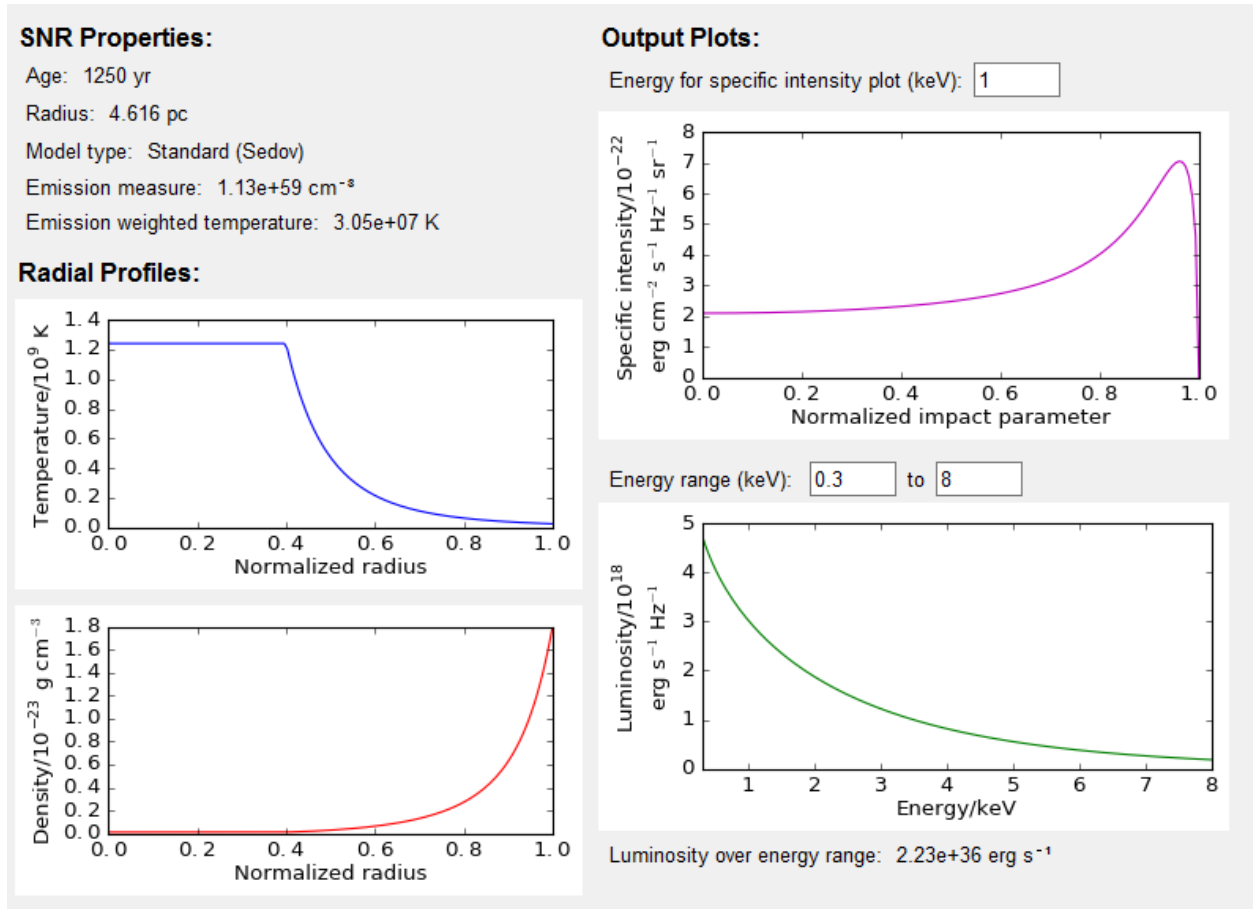


Fig. 5.— Screenshot of the Emissivity calculation tool of the SNR modelling program: For a SNR in the ST phase at age 1250 yr in a uniform CSM ($s=0$): radial profile of temperature (top left) and of density (bottom left). Surface brightness profile at 1 keV (top right panel) and spectrum integrated over the volume of the SNR (bottom right panel).

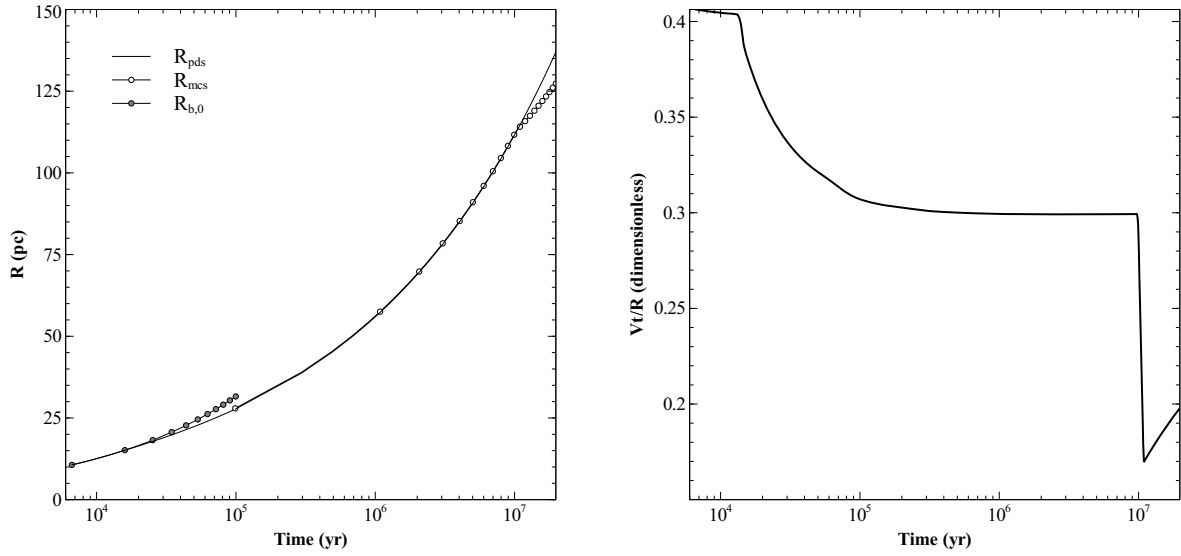


Fig. 6.— Left panel: Late-time evolution of blast-wave radius including transitions from ST to PDS and PDS to MCS phases. The line $R_{b,0}$ shows the ST evolution (up to 10^5 yr) without including transition to PDS phase; the line R_{pds} shows the PDS evolution without including transition to MCS phase; the line R_{mcs} includes the full evolution. Right panel: the deceleration index $m = Vt/R$ vs. time.

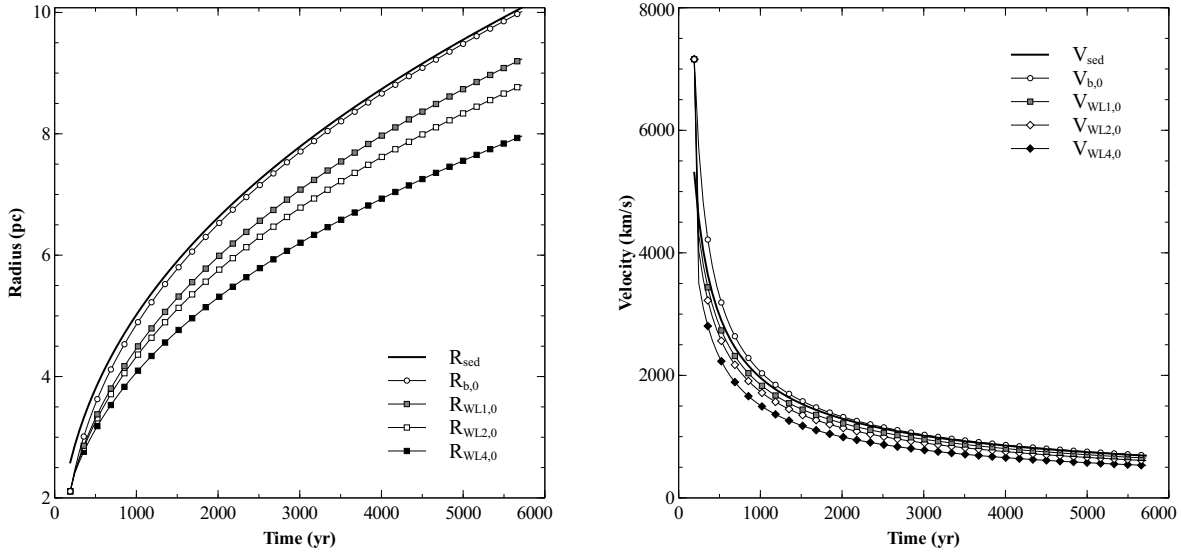


Fig. 7.— Comparison of SNR evolution in uniform ISM with SNR evolution in cloudy ISM . Left panel: comparison of of blast-wave radius for pure Sedov-Taylor (R_{sed}) and n=0 ST model ($R_{b,0}$) with cloudy ISM models with $C/\tau=1, 2$ and 4 , matched to the n=0 ST model ($R_{WL1,0}$, $R_{WL2,0}$ and $R_{WL4,0}$). The pure Sedov-Taylor solution and n=0 ST solutions have larger radius at all times than the solutions with cloudy ISM. Right panel: comparison of shock velocities for the same cases. The cloudy ISM models have shock velocity lower than the pure Sedov solution except at the very earliest times.

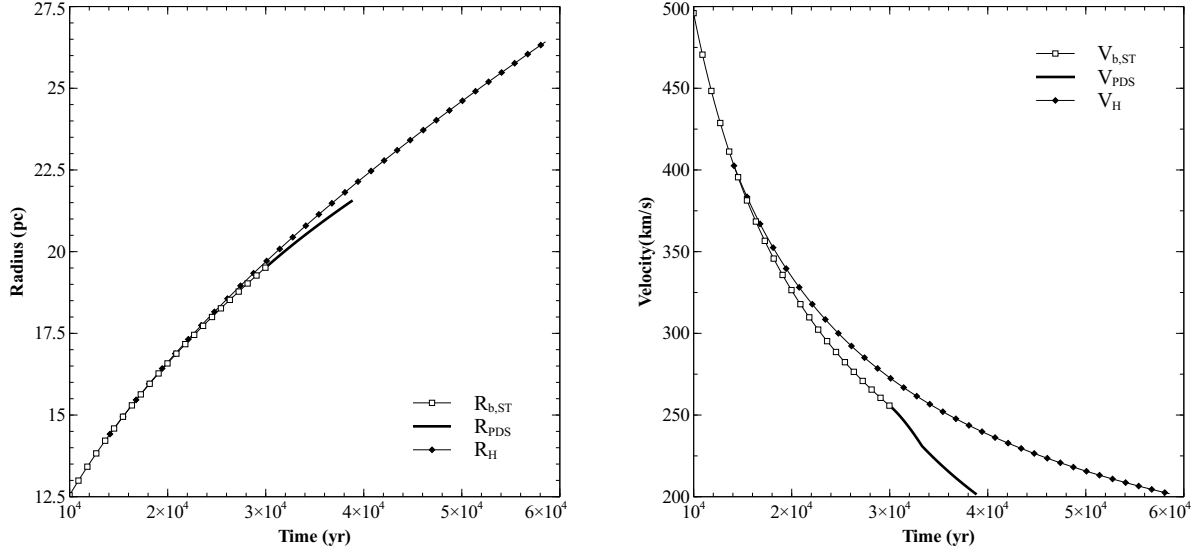


Fig. 8.— Left panel: Late-time evolution of blast-wave radius in a hot ISM ($T=10^6$ K). The lines $R_{b,ST}$ and R_{PDS} shows the standard evolution in ST and PDS phases up to merger at 3.87×10^4 yr. The line R_H shows the evolution including swept up thermal energy from the hot ISM. In the latter case merger occurs much later: at 5.85×10^4 yr. Right panel: the shock velocity for the standard evolution ($V_{b,ST}$ and R_{PDS}), and for the hot ISM model (V_H). Both models end with merger into the ISM at the same velocity.

Table 1. Dimensionless Emission Measures and Temperatures

phase	n	C/τ	dEM_f	dT_f	dEM_r	dT_r
Ejecta Dominated	7	n/a	0.753	1.228	0.611	0.538
Ejecta Dominated	12	n/a	0.916	1.129	11.82	0.119
Sedov	n/a	n/a	0.516	1.289	n/a	n/a
WL	n/a	1	0.774	1.370	n/a	n/a
WL	n/a	2	1.609	1.369	n/a	n/a
WL	n/a	4	6.932	1.383	n/a	n/a